# Design of electrically pumped nanolaser with metal–dielectric-metal coaxial ring cavity

# Design of electrically pumped nanolaser with metal–dielectric-metal coaxial ring cavity

Cite as: AIP Advances **10**, 105005 (2020); https://doi.org/10.1063/5.0023904
Submitted: 04 August 2020 . Accepted: 18 September 2020 . Published Online: 05 October 2020

Kuan-Ting Ho, Qian Ding, and Andreas Schenk

# Design of electrically pumped nanolaser with metal–dielectric-metal coaxial ring cavity

Cite as: AIP Advances 10, 105005 (2020); doi: 10.1063/5.0023904
Submitted: 4 August 2020 • Accepted: 18 September 2020 •
Published Online: 5 October 2020



Kuan-Ting Ho,[1,a] Qian Ding,[2,b] and Andreas Schenk[2,c]

## AFFILIATIONS

[1] Department of Materials Science and Engineering, EPFL, 1015 Lausanne, Switzerland
[2] Department of Information Technology and Electrical Engineering, ETH Zurich, 8092 Zurich, Switzerland

[a] **Electronic mail:** h.kuan.ting@gmail.com. **Now at:** Robert Bosch GmbH, 72762 Reutlingen, Germany.
[b] **Author to whom correspondence should be addressed:** dingq@iis.ee.ethz.ch
[c] **Electronic mail:** schenk@iis.ee.ethz.ch

## ABSTRACT

We employ self-consistently coupled opto-electrical simulations to explore the design strategy for a proposed electrically pumped metallic coaxial ring cavity nanolaser. With the optical cavity optimized to the physical size of $1.4(\lambda/n)^3$, the lasing ability using two gain medium schemes, bulk InGaAs and InGaAs/InP multiple quantum wells (MQWs), are compared. It is shown that the device with the bulk gain medium lases at 1568 nm, while the gain fails to overcome the optical loss in the case of the MQW gain medium due to its lower modal confinement ratio. Variations in material parameters like carrier mobility and Auger coefficient in the bulk laser or carrier capture time in the MQW laser are found to hardly change the lasing ability, although they do impact lasing threshold and efficiency in the bulk case. To study the possibility of further device down-scaling, the lasing feasibility of a smaller cavity with a size of $0.23(\lambda/n)^3$ is investigated. We demonstrate that neither including the Purcell effect nor using a metallic substrate for better mode confinement improves the lasing behavior.



## I. INTRODUCTION

Implementing highly integrated optical interconnect systems for chip-to-chip or board-to-board communication is believed to fulfill the increasing demand of high-speed data transfer with high throughput.[1] However, the miniaturization of one of the key components, i.e., laser sources, is restricted by the fundamental diffraction limit. To overcome this bottleneck, several approaches have been demonstrated.[2–4] One of the most promising is the metal-based plasmonic nanolaser.[5] Compared with conventional lasers designed with dielectric cavities, metal-based cavity lasers utilize plasmonic effects at the interface between the metal and the dielectric to confine light on the sub-wavelength scale and thus break the diffraction limit. Furthermore, to achieve ultimate compatible on-chip integration, it is necessary to design electrically pumped lasers that are under continuous operation at room temperature.[6] Although the metal cavity can serve as an electrical contact for carrier injection as well as a heat sink for stable operation, it is considered notorious for its high ohmic loss in optical devices. Therefore, the design of an electrically pumped metal cavity based plasmonic laser on the nanoscale still remains a challenge.

This work theoretically verifies the lasing feasibility of electrically pumped room-temperature plasmonic nanolasers with a coaxial ring cavity using either bulk InGaAs or InGaAs/InP multiple quantum wells (MQWs) as the gain medium. The designed laser structure is depicted in Fig. 1, based on the reported optically pumped nanolaser by Khajavikhan *et al.*[7] The laser cavity is built on a silicon dioxide substrate. The light is extracted from the top surface along the positive z-direction. Carriers are injected laterally between inner and outer metal rings, which form the coaxial cavity and serve as electrical contacts at the same time. Silver is chosen as the cavity material because of its small imaginary part of the

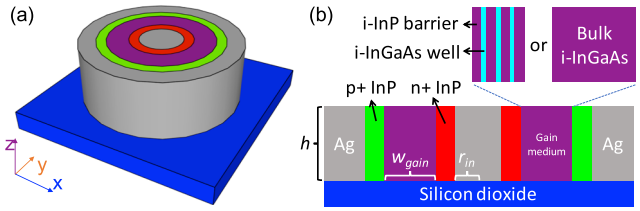


**FIG. 1**. (a) 3D schematic structure of the coaxial ring cavity nanolaser simulated in this work and (b) the schematic cross section of the cavity. The corresponding materials utilized and the varied geometry parameters, i.e., cavity height $h$, inner ring radius $r_{in}$, and gain medium width $w_{gain}$, are labeled.

permittivity resulting in a lower optical loss than gold.[8] Rings of heavily doped ($10^{19}$ cm$^{-3}$) n-type and p-type InP are used between the active gain medium and metal rings. The intrinsic gain medium is either bulk $In_{0.53}Ga_{0.47}As$ that is lattice-matched to InP or MQWs composed of 5 nm/10 nm $In_{0.53}Ga_{0.47}As$/InP as wells/barriers. Such a laterally arranged ring structure of quantum wells integrated on an SOI substrate can be fabricated using the template-assisted selective epitaxy (TASE) technology developed at IBM Europe, Zurich.[9] Similar, hexagonal-shaped, microdisk lasers with optical pumping have been demonstrated recently by Moselund's group.[10,11] One of the advantages of TASE compared to the more conventional wafer bonding method is the weaker temperature dependence of the lasers.

Coupled 2D opto-electrical simulations are performed to investigate the gain medium design strategy, where the simulation domain is given by the cross section shown in Fig. 1(b) (radial symmetry). The simulation flow runs as follows: First, the optical cavity is designed using *Lumerical finite-difference time-domain (FDTD)* to align its resonance wavelength with the spectrum of the gain medium. Each of its supported modes is characterized by five parameters comprising resonance wavelength, quality factor ($Q$), top-surface out-coupling loss quality factor ($Q_{out}$) for light extraction, confinement ratio ($\Gamma$), and modal optical profile. The obtained mode profile pattern together with the corresponding modal parameters then serve as the input to solve the electrical problem using the laser module of *Sentaurus Device*.[12] In this simulator, the quantum well (QW) is modeled as the recombination center in the frame of the drift-diffusion formalism follows the treatment mentioned by Grupen and Hess,[13] and the net characteristic capture time is set to 4 ps for both electrons and holes.[14,15] The gain calculation is based on Fermi's golden rule, where the QW subbands and wave functions are obtained using the analytical solutions of a simple finite-well model. The band offset at the InP/InGaAs interface is set to 0.105 eV /0.512 eV for $\Delta E_c/\Delta E_v$. Carrier pumping in barrier regions and polarization dependence of the QW gain are neglected in this model. The refractive index in *Lumerical* is then updated by an external calculation where free-carrier absorption,[16] band filling,[16] and band gap narrowing[17] are taken into account. Additional transport-relevant material properties are given as follows. The carrier mobilities in InP (InGaAs) are set to 5200 (14 000) cm$^2$/Vs for electrons and 170 (320) cm$^2$/Vs for holes with doping dependence included.[18] SRH lifetimes of 2(0.05) ns for electrons and 2(0.4) ns for holes are used in InP (InGaAs).[19,20] The Auger recombination coefficients are set to $10^{-31}$ cm$^6$/s in InP for both electrons and holes and to $10^{-31}/1.25 \times 10^{-29}$ cm$^6$/s for electrons/holes in InGaAs.[21] The impact of carrier mobility and Auger coefficient on the lasing characteristics of the bulk laser, as well as the influence of the carrier capture time on the lasing ability of the MQW laser, is studied in Sec. III.

During the device design phase in this work, the lattice temperature is assumed to be equal to room temperature (300 K). In order to mimic the temperature rise caused by self-heating and to further examine its impact on the lasing behavior, we perform additional isothermal simulations at elevated temperatures in the range of 400 K–500 K. This is done for the bulk device that successfully managed to lase at room temperature. The upper limit is chosen in virtue of the good thermal management provided by the metallic cavity. The highest lattice temperature due to self-heating in such devices has been reported to stay below 400 K in Ref. 22. The thermo-optical effect is taken into account by using a temperature-dependent refractive index in the optical simulation, with values reported in Ref. 23 for InP and linearly interpolated values for $In_{0.53}Ga_{0.47}As$ reported based on studies in Ref. 24 for InAs and Ref. 25 for GaAs. In general, this temperature dependence is very small for the studied III–V materials ($1.46 \times 10^{-4}$/K for InGaAs and $2.3 \times 10^{-4}$/K for InP). The thermo-electric impact is included by the temperature dependence of the transport parameters in the electrical simulations. For bandgap, effective density of states, and carrier mobility, available models in *Sentaurus Device* are employed. The temperature dependence of the Auger recombination coefficient in the bulk gain medium is calculated according to Ref. 26, where it slightly increases from $10^{-31}$ cm$^6$/s ($1.25 \times 10^{-29}$ cm$^6$/s) at 300K to $1.51 \times 10^{-31}$ cm$^6$/s ($1.87 \times 10^{-29}$ cm$^6$/s) at 400 K and $1.91 \times 10^{-31}$ cm$^6$/s ($2.83 \times 10^{-29}$ cm$^6$/s) at 500 K for electrons (holes). The temperature dependence of the SRH lifetimes is neglected here because, in lasers, SRH is much less important than Auger recombination. The latter has been identified as the main heat generation source, also in nanoscale lasers.[27] The results are discussed in Sec. III A.

## II. DESIGN OF THE CAVITY GEOMETRY

In order to maximize the lasing ability, the geometry of the optical cavity should be designed to support a high-$Q$ mode with its resonance wavelength aligned with the gain spectrum of the active medium. As seen from the gain spectrum in Fig. 2(a), the targeted resonance wavelength lies in the range of 1400 nm –1600 nm, where the gain of both cases, bulk and MQWs, is high enough. To start with, a large cavity is chosen in order to support a sufficient number of modes in the spectral range of interest, with its height, inner ring radius, InP contact, and active medium being 300 nm, 100 nm, 30 nm, and 190 nm, respectively. The label [$k$ $l$ $m$] is adopted to distinguish between different optical modes. The letter $k$/$m$ denotes the azimuthal/longitudinal mode number, whereas the letter $l$ clarifies the type of transverse mode: "$i$/$o$" stands for the plasmonic mode bound to the inner/outer ring surface, and "$w$" stands for the conventional whispering-gallery-like mode formed due to the high reflectivity of the metallic cavity. In our simulation, only modes with $k$ equal to 0 are selected because of the radial symmetry requirement in our setting in *Sentaurus Device*. The profiles of the transverse

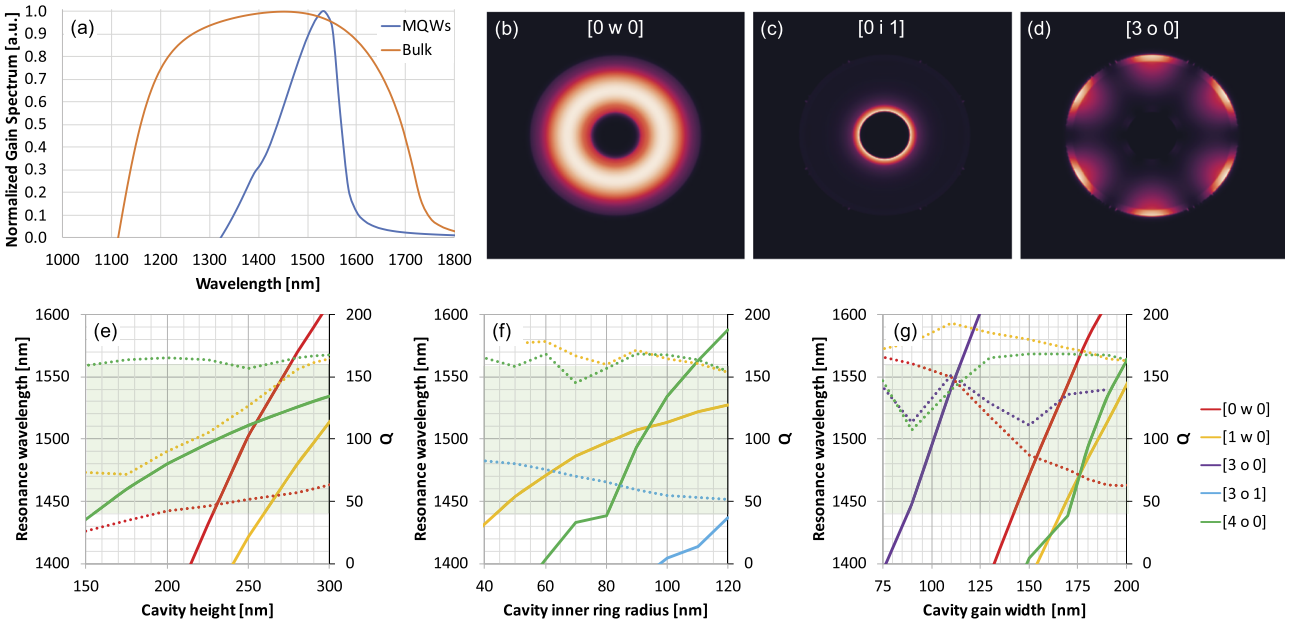


**FIG. 2**. (a) Normalized gain spectrum of bulk and MQW gain medium, the transverse intensity profiles of three supported modes (b) [0 *w* 0], (c) [0 *i* 1], and (d) [3 *o* 0], and modal resonance wavelength (solid line) and Q-factor (dashed line) shift over (e) cavity height, (f) cavity inner ring radius, and (g) cavity gain width.

intensity of three supported modes, [0 *w* 0], [0 *i* 1], and [3 *o* 0], are given in Figs. 2(b)–2(d) to illustrate the used naming rule.

Three most crucial geometry parameters of the coaxial cavity, namely, its height, its inner ring radius, and the width of the gain medium, are varied to study their impact on resonance wavelength and the Q-factor of the supported modes. The results are shown in Figs. 2(e)–2(g), where only modes with a resonance wavelength in our targeted spectral range are plotted, and the spectral range of the MQW gain medium is highlighted in the green area. First, it can be seen that the resonance wavelength generally decreases when these three geometrical parameters are scaled down. Second, the dependence of the Q-factor on the geometry varies from mode to mode. The observed fluctuation of the Q-factor as a function of geometry parameters results from the mode overlapping in the FDTD simulation which prevents a more accurate determination of *Q*. Third, it is clear that the number of modes reduces when the cavity size decreases or when the MQW gain medium is used.

## III. DESIGN OF THE GAIN MEDIUM: BULK VS MQW

Given the design principle for the cavity outlined in the last section, we choose a cavity with a height/inner ring radius/gain width of 300 nm/100 nm/190 nm and mode [0 *w* 0] for the following design study of the gain medium. The physical cavity size is equal to $1.4(\lambda/n)^3$. The laser performance for the two cases, bulk InGaAs and InGaAs/InP MQWs (12 well/barrier pairs) as the gain medium, is simulated to find out the better design by comparison. The modal parameters and the results of the laser simulation at a forward bias of 3 V are listed in Table I. As can be seen, the nanolaser is able to lase only in the first case (bulk InGaAs gain medium). In the second case (MQW gain medium), the insertion of the InP barriers shrinks the active region, which reduces the confinement ratio. As a result, the modal gain of the MQW medium is lower than the one for the bulk gain medium, and lasing becomes more difficult.

### A. Bulk laser

The *LI*-curve and differential quantum efficiency (diff. QE) for the bulk laser are shown as red-colored curves in Fig. 3(a). Its lasing threshold current is ~3.5 mA with an external quantum efficiency of ~0.47%. This high threshold current is a consequence of the low Q-factor, which demands a higher injection level to obtain a larger modal gain. The low quantum efficiency is related to the high optical loss. Considering the possible variations in material parameters, the lasing properties with lower carrier mobilities

**TABLE I**. The modal parameters and the results of laser simulation at a forward bias of 3 V.

| | Bulk InGaAs | InP/InGaAs MQW |
|---|---|---|
| Resonance wavelength (nm) | 1568 | 1493 |
| $Q$ | 73 | 62 |
| $Q_{out}$ | 606 | 516 |
| $\Gamma$ (%) | 64 | 21 |
| Modal gain [1/ps] | 0.824 | 0.313 |
| Cavity loss [1/ps] | 0.415 | 0.515 |

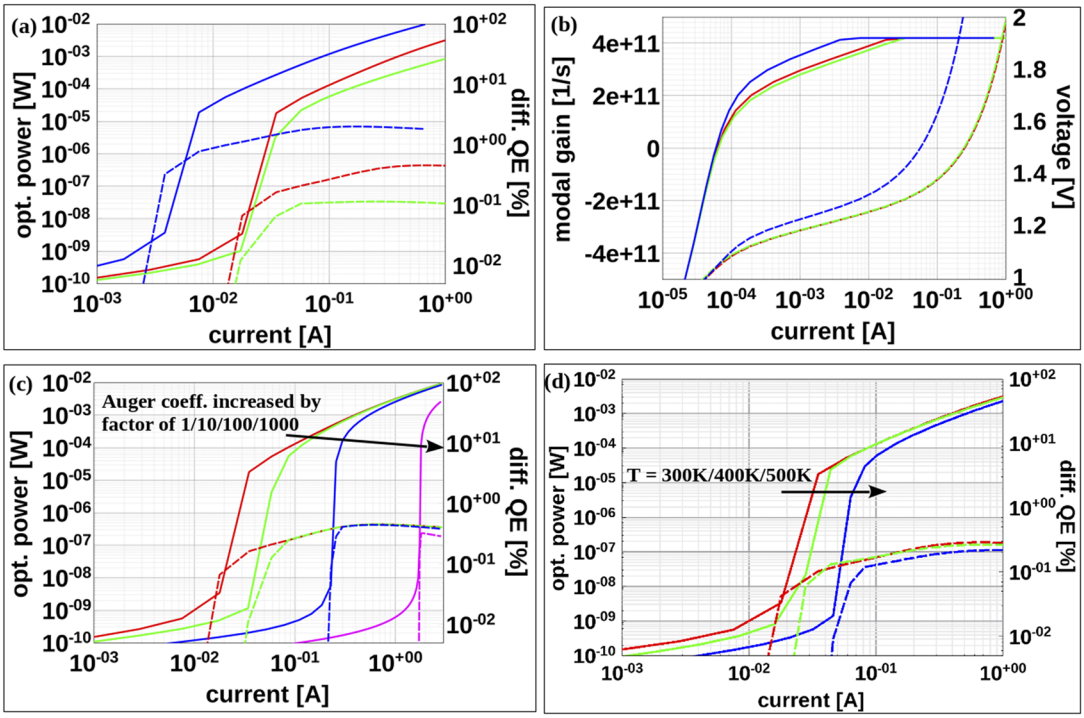


**FIG. 3**. Bulk laser with a cavity height/inner ring radius/gain width of 300 nm/100 nm/190 nm: (a) *LI*-curves (solid lines) in the log–log scale and diff. QE vs current curves (dashed lines) with unscaled (red) and reduced electron(blue)/hole(green) mobility by a factor of 5, (b) modal gain vs current curves (solid lines) and *VI*-curves (dashed lines) corresponding to the 3 cases in (a), (c) *LI*-curves (solid lines) in the log–log scale and diff. QE vs current curves (dashed lines) with upscaled Auger recombination coefficients by a factor of 1(red)/10(green)/100(blue)/1000(magenta), and (d) *LI*-curves (solid lines) in the log–log scale and diff. QE vs current curves (dashed lines) with a uniform device temperature of 300 K(red)/400 K(green)/500 K(blue).

[Fig. 3(a)] or a higher Auger recombination coefficient [Fig. 3(c)] are studied additionally. As for the carrier mobilities, it can be seen from Fig. 3(a) that the threshold current increases and the diff. QE decreases with a lower hole mobility (reduced by a factor of 5) as expected, while the opposite trend is observed for electrons. The reason for the lower threshold current with a reduced electron mobility is qualitatively explained in Fig. 3(b). First, at a given voltage below the lasing threshold, reducing the electron mobility results in a much lower current than reducing that of holes [dashed curves in Fig. 3(b)] due to the much higher mobility of electrons. In other words, to reach the same current level, the bias has to be higher with a lower electron mobility. On the other hand, a higher bias means a larger energy splitting between the Fermi levels of electrons and holes, which results in a higher stimulated emission rate and, thus, a higher modal gain, as seen from the solid curves in Fig. 3(b). Therefore, less current is needed to reach the lasing threshold. Since a higher gain is equivalent to a higher output optical power at the same current level, the diff. QE is hence higher due to its proportionality to the slope of the *LI*-curve. As for the Auger recombination coefficient, it is increased by factors of 10, 100, and 1000 to study its impact on the lasing properties. Figure 3(c) shows that the lasing ability is still robust and the diff. QE remains almost the same even when the Auger coefficient is upscaled by 3 orders of magnitude. However, the threshold current increases by orders of magnitude, which is also well known for conventional large lasers.[28,29]

The device temperature not only affects the material parameters but also has a strong influence on the lasing properties in both traditional large lasers[30,31] and recently reported nanolasers.[32,33] Here, we study the thermal effect on lasing threshold and diff. QE of the bulk laser by comparing simulations at 300 K, 400 K, and 500 K, respectively. The results are depicted in Fig. 3(d). As can be seen, its lasing ability is quite robust up to 500 K, but the threshold current increases by roughly a factor of 3 when a uniform temperature increase of 200 K is assumed. The diff. QE starts to drop at 500 K due to the stronger Auger recombination at higher temperature. The higher threshold current caused by the lattice heating leads to an increased power consumption of the device. It also indicates that the device could potentially fail to lase when further scaled down. All these negative impacts impose additional obstacles to achieving monolithically integrated low-power optical links.

## B. MQW laser

MQW gain mediums have been widely used in conventional laser design for large structures to reduce the lasing threshold because of their higher differential material gain than a bulk gain medium.[34,35] In fact, we can see in our results that the modal gain per

1% confinement ratio is indeed higher for the MQW gain medium (0.0149 $ps^{-1}$/1% Γ) than the bulk (0.0129 $ps^{-1}$/1% Γ) gain medium at 3 V, implying a higher carrier recombination efficiency for the MQW gain medium. However, due to the high optical loss in small cavities, the confinement ratio becomes more sensitive to the gain medium and, therefore, turns out to be an important factor in determining the lasing ability of nanoscale lasers. As seen in Table I, the modal gain scales down with approximately the same factor as the confinement factor, making it difficult to overcome the loss. Taking into account possible variations of the carrier capture time used in the quantum well laser model, we also checked the lasing ability with a capture time 10-times shorter (0.4 ps). Although the faster carrier capture process results in a bit higher modal gain, 0.381/ps compared with the original 0.313/ps at 3 V listed in Table I, it is still far from sufficient to compensate the reduction of modal gain caused by the low confinement ratio of the MQW laser.

## IV. EFFECT OF FURTHER DOWN-SCALING

An even smaller nanolaser boosts the possibility of opto-electrical integration. In principle, small cavities could benefit more from the Purcell effect, where the spontaneous and stimulated emission might be enhanced due to the increased optical density of state.[36] Furthermore, the small cavity increases the possibility for single-mode lasing, where the spontaneous emission coupling factor $\beta$ is close to unity and potentially reduces the threshold.[37] Here, we study the lasing feasibility of a smaller nanolaser with both bulk and MQW gain mediums by evaluating the Purcell effect and implementing a metal substrate. A cavity size of a height/inner ring radius/InP contact width/gain width of 165 nm/100 nm/20 nm/55 nm and mode [0 $i$ 1] is chosen for this study. The physical cavity size equals $0.23(\lambda/n)^3$.

### A. Purcell effect

The Purcell enhancement factor is proportional to the full width at half maximum of the gain spectrum and inversely proportional to the effective model volume ($V_{\text{eff}}$) when the gain spectrum is broader than the modal spectrum.[38] This effect is included in the simulation framework by multiplying the original modal gain, i.e., emission rates, with a modified Purcell factor ($F_{\text{p}}$), which is estimated by

$$F_{\text{p}} = \frac{3}{4\pi^2}\left(\frac{\lambda}{n}\right)^3 \frac{Q_{\text{gain}}}{V_{\text{eff}}}, \tag{1}$$

where $\lambda$ is the resonance wavelength, $n$ is the refractive index of the gain medium, and $Q_{\text{gain}}$ is the Q-factor of the gain spectrum calculated as the full width at half maximum of the gain spectrum divided by the modal resonance frequency. The original Q-factor of the cavity is replaced by $Q_{\text{gain}}$ in this estimation due to the fact that the emitter line width is generally wider than the cavity line width in the case of the bulk or the MQW gain medium.[39] Modal parameters, Purcell factor, and results of the laser simulation at a bias of 3 V are listed in Table II. For the bulk gain medium, the Purcell factors are smaller than 1, meaning no emission is enhanced. For the MQW gain medium, the emission is enhanced by a factor of 3.71, but the modal gain still cannot overcome the cavity loss due to the inherently low confinement ratio. This indicates the difficulty of designing true nanoscale lasers after including the commonly neglected Purcell effect for the bulk or the MQW gain medium.

**TABLE II**. Simulation results for the smaller cavity at a bias of 3 V.

| | Bulk InGaAs | InP/InGaAs MQW |
|---|---|---|
| Resonance wavelength (nm) | 1494 | 1488 |
| $Q$ | 41 | 37 |
| $Q_{\text{out}}$ | 446 | 403 |
| Γ (%) | 45 | 12 |
| $Q_{\text{gain}}$ | 2.55 | 11.23 |
| $F_{\text{p}}$ | 0.84 | 3.71 |
| Modal gain [1/ps] | 0.165 | 0.141 |
| Cavity loss [1/ps] | 0.789 | 0.876 |

### B. Effect of the metal substrate

A metal substrate is able to block the out-coupling into the substrate and theoretically increase the cavity Q-factor, thus enhancing the lasing ability of the nanolaser. A modified substrate design with

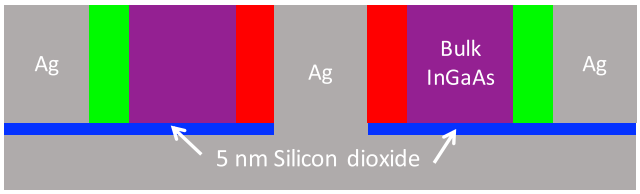


**FIG. 4**. Cross section of the coaxial ring cavity on a metal substrate separated by a thin silicon dioxide layer and the materials utilized.

**TABLE III**. The mode parameters of the [0 $i$ 1] mode in the small cavity with and without the metal substrate.

| | Without the metal substrate | With the metal substrate |
|---|---|---|
| Top view |  |  |
| Side view | 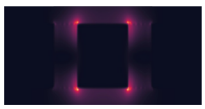 | 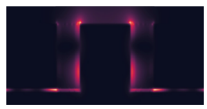 |
| Resonance wavelength (nm) | 1487 | 1088 |
| $Q$ | 40.08 | 46.21 |
| $Q_{\text{out}}$ | 442.8 | 386.5 |
| Γ (%) | 45 | 38 |

silver is depicted in Fig. 4. The inner metal ring directly is in contact with the metal substrate, whereas the outer metal ring is separated from the metal substrate by a 5 nm thick silicon dioxide layer to avoid short circuiting of the device.

The modal parameters of the [0 $i$ 1] mode in the small cavity with and without the metal substrate are listed in Table III. The modal optical profile is pushed upward by the metal substrate, and the resonance wavelength is blue-shifted. The Q-factor of the cavity with the metal substrate increases as desired, but only by 15.3% due to additional plasmonic loss, which on the other hand leads to a decrease in the confinement ratio by 7%. Thus, the overall enhancement of the modal parameters and the implied lasing ability for the studied mode of the chosen cavity size is small.

## V. CONCLUSION

We theoretically demonstrated the lasing ability of a coaxial ring nanolaser with a bulk InGaAs gain medium at room temperature using electrical pumping. With the cavity height/inner ring radius/gain region width designed as 300 nm/100 nm/190 nm, a whispering-gallery-like mode [0 $w$ 0] with a wavelength of about 1550 nm could lase. It has also been shown that owing to the low confinement ratio, a cavity of the same size but with an InGaAs(5 nm)/InP(10 nm) MQW gain medium is rather inadequate to lase. This conclusion remains unaltered when lowering the carrier mobility by a factor of 5, increasing the Auger coefficient by up to 3 orders of magnitude, or increasing the device temperature uniformly to 500 K in the bulk laser and using a carrier capture time 10-times shorter in the MQW laser. We further explored the lasing ability of a true nanoscale laser with a physical cavity size of $0.23(\lambda/n)^3$ by evaluating the Purcell effect and implementing a metal substrate. We found that for the studied [0 $i$ 1] mode, a Purcell enhancement is achieved only in the case of the MQW gain medium and that the modal gain can still hardly overcome the cavity loss for both bulk and MQWs gain media. When using a metallic substrate, an additional plasmonic loss is induced which reduces the confinement ratio and limits the improvement of the Q-factor. Therefore, the overall improvement might be insufficient to leverage lasing in the studied nanoscale cavity.

## DATA AVAILABILITY

The data that support the findings of this study are available from the corresponding author upon reasonable request.

## REFERENCES

[1] C.-Z. Ning, "Semiconductor nanolasers and the size-energy-efficiency challenge: A review," Adv. Photonics **1**, 1 (2019).
[2] S. L. McCall, A. F. J. Levi, R. E. Slusher, S. J. Pearton, and R. A. Logan, "Whispering-gallery mode microdisk lasers," Appl. Phys. Lett. **60**, 289–291 (1992).
[3] Y. Zhang, C. Hamsen, J. T. Choy, Y. Huang, J.-H. Ryou, R. D. Dupuis, and M. Loncar, "Photonic crystal disk lasers," Opt. Lett. **36**, 2704–2706 (2011).
[4] Y. Ma, X. Guo, X. Wu, L. Dai, and L. Tong, "Semiconductor nanowire lasers," Adv. Opt. Photonics **5**, 216–273 (2013).
[5] S. Gwo and C. K. Shih, "Semiconductor plasmonic nanolasers: Current status and perspectives," Rep. Prog. Phys. **79**, 086501 (2016).
[6] M. T. Hill, "Electrically pumped metallic and plasmonic nanolasers," Chin. Phys. B **27**, 114210 (2018).
[7] M. Khajavikhan, A. Simic, M. Katz, J. H. Lee, B. Slutsky, A. Mizrahi, V. Lomakin, and Y. Fainman, "Thresholdless nanoscale coaxial lasers," Nature **482**, 204–207 (2012).
[8] P. B. Johnson and R. W. Christy, "Optical constant of the nobel metals," Phys. Rev. B **6**, 4370–4379 (1972).
[9] H. Schmid, M. Borg, K. Moselund, L. Gignac, C. M. Breslin, J. Bruley, D. Cutaia, and H. Riel, "Template-assisted selective epitaxy of III–V nanoscale devices for co-planar heterogeneous integration with Si," Appl. Phys. Lett. **106**, 233101 (2015).
[10] S. Mauthe, B. Mayer, M. Sousa, G. Villares, P. Staudinger, H. Schmid, and K. Moselund, "Monolithically integrated InGaAs microdisk lasers on silicon using template-assisted selective epitaxy," Proc. SPIE **10672**, 150–158 (2018).
[11] S. Mauthe, N. Vico Triviño, Y. Baumgartner, M. Sousa, D. Caimi, T. Stöferle, H. Schmid, and K. E. Moselund, "InP-on-Si optically pumped microdisk lasers via monolithic growth and wafer bonding," IEEE J. Sel. Top. Quantum Electron. **25**, 1–7 (2019).
[12] Synopsys, *Sentaurus Device User Guide* (Synopsys Inc., 2006), p. 1488.
[13] M. Grupen and K. Hess, "Simulation of carrier transport and nonlinearities in quantum-well laser diodes," IEEE J. Quantum Electron. **34**, 120–140 (1998).
[14] D. J. Westland, D. Mihailovic, J. F. Ryan, and M. D. Scott, "Optical time-of-flight measurement of carrier diffusion and trapping in an InGaAs/InP heterostructure," Appl. Phys. Lett. **51**, 590–592 (1987).
[15] R. Kersting, X. Q. Zhou, K. Wolter, D. Grützmacher, and H. Kurz, "Subpicosecond luminescence study of carrier transfer in InGaAs/InP multiple quantum wells," Superlattices Microstruct. **7**, 345–348 (1990).
[16] B. R. Bennett, R. A. Soref, and J. A. Del Alamo, "Carrier-induced change in refractive index of InP, GaAs, and InGaAsP," IEEE J. Quantum Electron. **26**, 113–122 (1990).
[17] S. C. Jain, J. M. McGregor, and D. J. Roulston, "Band-gap narrowing in novel III–V semiconductors," J. Appl. Phys. **68**, 3747–3749 (1990).
[18] M. Sotoodeh, A. H. Khalid, and A. A. Rezazadeh, "Empirical low-field mobility model for III–V compounds applicable in device simulation codes," J. Appl. Phys. **87**, 2890–2900 (2000).
[19] J. W. Parks, A. W. Smith, K. F. Brennan, and L. E. Tarof, "Theoretical study of device sensitivity and gain saturation of separate absorption, grading, charge, and multiplication InP/InGaAs avalanche photodiodes," IEEE Trans. Electron Devices **43**, 2113–2121 (1996).
[20] H. W. Chiang, J. C. Rode, P. Choudhary, and M. J. Rodwell, "Lateral carrier diffusion and current gain in terahertz InGaAs/InP double-heterojunction bipolar transistors," J. Appl. Phys. **115**, 1–4 (2014).
[21] J. M. López-González and L. Prat, "Numerical modelling of abrupt InP/InGaAs HBTs," Solid-State Electron. **39**, 523–527 (1996).
[22] J. Shane, Q. Gu, F. Vallini, B. Wingad, J. S. T. Smalley, N. C. Frateschi, and Y. Fainman, "Thermal considerations in electrically-pumped metallo-dielectric nanolasers," Proc. SPIE **8980**, 500–510 (2014).
[23] E. Gini and H. Melchior, "Thermal dependence of the refractive index of InP measured with integrated optical demultiplexer," J. Appl. Phys. **79**, 4335–4337 (1996).
[24] G. D. Gillen, C. DiRocco, P. Powers, and S. Guha, "Temperature-dependent refractive index measurements of wafer-shaped InAs and InSb," Appl. Opt. **47**, 164–168 (2008).
[25] J. P. Kim and A. M. Sarangan, "Temperature-dependent Sellmeier equation for the refractive index of $Al_xGa_{1-x}As$," Opt. Lett. **32**, 536–538 (2007).
[26] P. Rees, P. Blood, M. J. H. Vanhommerig, G. J. Davies, and P. J. Skevington, "The temperature dependence of threshold current of chemical beam epitaxy grown InGaAs–InP lasers," J. Appl. Phys. **78**, 1804–1807 (1995).
[27] A. A. Vyshnevyy and D. Y. Fedyanin, "Self-heating induced bistability in metal-clad semiconductor nanolasers," in *Advanced Photonics 2018 (BGPP, IPR, NP, NOMA, Sensors, Networks, SPPCom, SOF)* (Optical Society of America, 2018).
[28] A. Sugimura, "Band-to-band Auger recombination effect on InGaAsP laser threshold," IEEE J. Quantum Electron. **17**, 627–635 (1981).

[29]R. Fehse, S. Tomic, A. R. Adams, S. J. Sweeney, E. P. O'Reilly, A. Andreev, and H. Riechert, "A quantitative study of radiative, Auger, and defect related recombination processes in 1.3-$\mu$m GaInNAs-based quantum-well lasers," IEEE J. Sel. Top. Quantum Electron. **8**, 801–810 (2002).
[30]J. Pankove, "Temperature dependence of emission efficiency and lasing threshold in laser diodes," IEEE J. Quantum Electron. **4**, 119–122 (1968).
[31]P. P. Baveja, B. Kögel, P. Westbergh, J. S. Gustavsson, Å. Haglund, D. N. Maywar, G. P. Agrawal, and A. Larsson, "Assessment of VCSEL thermal rollover mechanisms from measurements and empirical modeling," Opt. Express **19**, 15490–15505 (2011).
[32]Q. Gu, J. S. T. Smalley, J. Shane, O. Bondarenko, and Y. Fainman, "Temperature effects in metal-clad semiconductor nanolasers," Nanophotonics **4**, 26–43 (2015).
[33]Y. Fan and K. A. Shore, "Design of room temperature electrically pumped visible semiconductor nanolasers," IEEE J. Quantum Electron. **54**, 1–7 (2018).
[34]M. Asada, A. Kameyama, and Y. Suematsu, "Gain and intervalence band absorption in quantum-well lasers," IEEE J. Quantum Electron. **20**, 745–753 (1984).
[35]M. Rosenzweig, M. Möhrle, H. Düser, and H. Venghaus, "Threshold-current analysis of ingaas-ingaasp multiquantum well separate-confinement lasers," IEEE J. Quantum Electron. **27**, 1804–1811 (1991).
[36]K. J. Vahala, "Optical microcavities," in *2005 European Quantum Electronics Conference, EQEC '05* (IEEE, 2005), Vol. 2005, p. 352.
[37]R.-M. Ma and R. F. Oulton, "Applications of nanolasers," Nat. Nanotechnol. **14**, 12–22 (2019).
[38]B. Romeira and A. Fiore, "Purcell effect in the stimulated and spontaneous emission rates of nanoscale semiconductor lasers," IEEE J. Quantum Electron. **54**, 1–12 (2018); arXiv:1801.08879.
[39]B. Romeira and A. Fiore, "Purcell effect in the gain and spontaneous emission of nanolasers," in *Conference Digest - IEEE International Semiconductor Laser Conference* (IEEE, 2016), pp. 1–2.